COBEM 2023 27TH INTERNATIONAL CONGRESS OF MECHANICAL ENGINEERING

ABCM Brazilian Society of Mechanical Sciences and Engineering
27th ABCM International Congress of Mechanical Engineering
December 04-08, 2023, Florianópolis-SC, Brazil

COB-2023-1365
MODELING AND SIMULATION OF GREEN HYDROGEN GENERATION – A REVIEW

Roque Martins Duarte Junior[1]
Rômulo Luis de Paiva Rodrigues[2]
Janine Padilha Botton[3]
Cezar Otaviano Ribeiro Negrão[4]
[1,2,4] Research Center for Rheology and Non-Newtonian Fluids (CERNN)
Postgraduate Program in Mechanical and Materials Engineering (PPGEM)
Federal University of Technology – Paraná (UTFPR)
R. Deputado Heitor Alencar Furtado, 5000, CEP: 81280-340 Curitiba, PR, Brazil.
roquemdjunior@gmail.com[1], romulorodrigues@utfpr.edu.br[2], negrao@utfpr.edu.br[4].

[3] Federal University of Latin American Integration.
Tancredo Neves Av., 6731, UNILA, Block 6, E3S11.CEP: 85867970 - Foz do Iguaçu, PR, Brazil
janine.padilha@unila.edu.br

Abstract. *There has been an energy transition to renewable sources with a focus on zero carbon emissions due to climate change and the global need to reduce carbon dioxide emissions. Among these clean energy options, green hydrogen appears as a good energy vector because it has a high calorific value and does not pollute. Green hydrogen generation occurs via water electrolysis and the most developed commercial technology available for industrial application is alkaline, it has good durability and low specific costs. However, this technology features a low current density value and gas transmission through the membrane during dynamic operating conditions, which may result in a mixture of flammable gases and generate serious problems. One way to analyze the operation of these electrolyzers is through modeling and simulation, considering reviewed alkaline water electrolysis modeling from the perspective of thermodynamic, electrochemical, thermal, and gas purity. Several authors have proposed models on this topic, but due to its complexity, more studies are required. Therefore, this paper aims to provide a review of the works in the literature on modeling and simulating hydrogen via alkaline electrolysis, especially on the studies that modeled and validated through experimental work.*

Keywords: *green hydrogen generation, modeling, simulation, water electrolysis.*

1. INTRODUCTION

Global concern has increased about higher levels of carbon dioxide (CO2) emissions and global warming, as a consequence, it has led governments to invest in new energy sources in the energy mix, mainly clean and renewable energy.

The renewable sources that grew the most in the last decade were solar and wind energy, however, they are naturally intermittent, and this has generated significant problems for electrical system operators. In addition, with the expectation of increasing investment in solar and wind, these problems are expected to enhance even more.

One solution to the intermittency problem is green hydrogen (H2), a high energy density that does not emit greenhouse gases. H2 has received great attention in recent years and is considered a promising energy carrier for the future.

Green hydrogen is obtained by water electrolysis, an efficient process to produce clean hydrogen with a purity higher than 99%. Alkaline water electrolysis (AWE) has a relatively stable and mature technology used in industrial applications. AWE is considered one of the most reliable technologies for producing green hydrogen (Jang et al., 2021).

Despite being consolidated in the market, this technology has problems such as low current density and gas transfer through the membrane under dynamic operating conditions, which can generate a flammable mixture and cause serious problems.

One way to better understand the operation and functioning of this technology is through numerical modeling and simulation. A literature review verified that although authors develop numerical studies of this equipment, they do not consider the internal components of the cell, such as pre-electrode, electrode, membrane, and gas chamber, nor the influence caused by these components.

Therefore, this article proposes to review the detailed literature on modeling and numerical simulation, focusing on works that implemented geometric aspects in simulations.

2. MODELING AND SIMULATION REVIEW

To facilitate the understanding of the modeling and simulation of the multiple physical processes that occur in the AWE, it is divided into the following topics: thermodynamics, electrochemistry, thermal, and purity of gases, as shown in Figure 1.

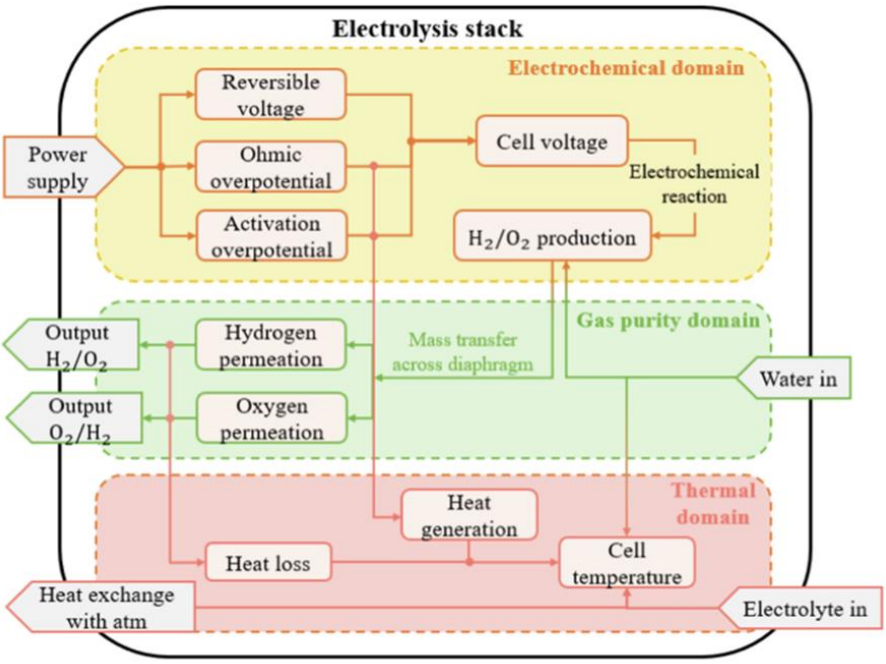

Figure 1 – Multiple systems divided in mathematical modeling as electrochemical (Hu et al., 2022).

The thermodynamic part evaluates the properties of the substances involved in the internal reactions, electrochemistry models the electrochemical domain by evaluating the cell voltage, gas production, reversible voltage, and ohmic and activation overpotential. Thermal assesses internal temperature change, heat generation, and heat loss, and lastly, gas purity studies mass transfer through the diaphragm and permeability of hydrogen and oxygen.

2.1 THERMODYNAMICS

Thermodynamics analyzes equilibrium reactions considering the thermal effects. This approach helps in defining the driving forces during the transport phenomena of reactions that occur in the electrolyte and in the description of electrolyte properties (Hammoudi et al., 2012). In these models, the Gibbs free energy equation (G), reversible voltage, and the cell's real voltage (thermoneutral) are used, with the reversible voltage considering the variation of G, and the thermoneutral enthalpy variation.

The equations that dictate this modeling are shown in Eq. 1, Eq. 2, and Eq. 3.

$$\Delta G = \Delta H - Q = \Delta H - T\Delta S \tag{1}$$

$$V_{rev} = \frac{\Delta G}{n \bullet F} \tag{2}$$

$$V_{tn} = \frac{\Delta H}{n \bullet F} \tag{3}$$

where ΔS represents the entropy change, T is the temperature of the reaction, n is the charge transferred for producing 1 mol of hydrogen (n = 2), and F represents the constant of Faraday (F = 96485 C/mol). For the water electrolysis, the Gibbs free energy is 237 kJ/mol, and the enthalpy 286 kJ/mol at 298 K and 1 bar (standard condition) under the assumed hypothesis of hydrogen and oxygen being ideal gases, water as an incompressible fluid, and the gaseous and liquid being separated phases.

According to Zeng and Zhang (2010), the enthalpy is little affected by temperature, while the operating temperature together with entropy (referring to the G equation) are greatly influenced by temperature so that the reversible voltage is more sensitive to temperature than the thermoneutral voltage.

2.2 ELECTROCHEMICAL

Lee et al. (2021) developed a three-dimensional (3D) transient numerical model of an alkaline water electrolysis (AWE) cell with potassium hydroxide solution as the working fluid. The model is experimentally validated with a range of currents as high as 2.0 A/m². The quantitative losses were investigated to include porous electrodes and a porous separator effect at low and high electrolyte flow rates. A fundamental understanding of the electrochemical and transport phenomena is provided by the current comprehensive 3-D AWE model, which may also be used to develop large-scale AWE cell and stack geometries for grid-scale hydrogen production.

Hu et al. (2022) reviewed the mathematical modeling work of alkaline electrolysis systems (AWE) and discusses the precision and calibration of thermodynamic and mechanism models of AWE electrochemical, as well as the extension of the mechanism model of thermal from the stack to the system. The authors classify the existing technologies in alkaline water electrolysis (AWE), proton exchange diaphragm water electrolysis (PEM), and solid oxide electrolysis cell (SOEC). The authors present Figure 2, shown below, highlighting the characteristics and operating conditions that influence each component of the electrochemical domain models. For the reversible voltage component, the operating conditions that influence are temperature, pressure, and electrolyte concentration. The ohmic overpotential component is influenced by characteristics of the electrode gap, diaphragm porosity, tortuosity, and bubble coverage rate, and also by the operating conditions such as the temperature, pressure, electrolyte concentration, and electrolyte flow rate. Besides that, the activation overpotential is varied by the characteristics of the electrode material and bubble coverage rate, and also by the operating conditions factors of temperature, pressure, and current exchange density.

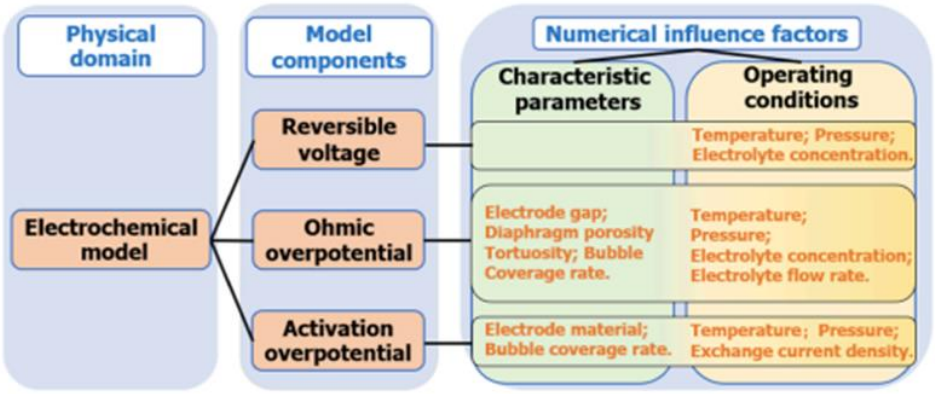

Figure 2. Electrochemical model guide (Hu et al., 2022).

The reversible voltage is calculated by the Nernst Equation indicated below.

$$V_{rev} = V_{rev}^{0} + \frac{R \bullet T}{2F} \ln\left(\frac{P_{H_2} \bullet P_{O_2}^{0.5}}{\alpha_{H_2O}}\right) \quad (1)$$

where R is the gas constant, P_{H2} indicates the partial pressures of hydrogen and the P_{O2} of oxygen. In Eq. 1, the first term is the standard reversible voltage V_{rev}^{0}, and the second term is the contribution due to the operating conditions.

Considering the partial pressure of impurity gas is negligible, water vapor in the gas is saturated, and the pressure on both sides of the cathode and anode is equal, resulting in Eq. (2).

$$V_{rev} = V_{rev}^{0} + \frac{R \bullet T}{2F} \ln\left[\frac{(P - P_{H_2O})^{1.5}}{\alpha_{H_2O}}\right] \quad (2)$$

where α_{H2O} is the water activity.

The equation of the activation overpotential is derived from the Butler-Volmer equation, it can be.

$$J = J_{0,k}\left[\frac{C_{PE}}{C_{PS}} \bullet \exp\left(\frac{n \bullet \alpha_k \bullet F \bullet V_{act,k}}{R \bullet T}\right) - \frac{C_{RE}}{C_{RS}} \bullet \exp\left(\frac{-n \bullet (1-\alpha_k) \bullet F \bullet V_{act,k}}{R \bullet T}\right)\right] \quad (3)$$

where C_{PE} means the concentration of substance P on the electrolyte and C_{PS}on the electrode surface, C_{RE} represent the concentration of substance R on the electrolyte and C_{RS} on the electrode surface, $J_{0,k}$ is the exchange current density of electrode k, and α_k represents the charge transfer coefficient.

The simplification of the activation overpotential is obtained considering that the concentration of each substance is usually assumed to be the same at different places, it means that $C_{PE} = C_{PS}$, $C_{RE} = C_{RS}$, and the charge transfer coefficients of cathode and anode are equal, as $\alpha_a = \alpha_c = 0{,}5$. Therefore, the activation overpotential is showed as below:

$$V_{act,k} = \frac{R \bullet T}{F} \sin^{-1}\left(\frac{J}{2J_{0,k}}\right) \tag{4}$$

The value of the second term in Eq. 3 is quite small when the reaction is at a high current density. Thus, the second term can be neglected, and the activation overpotential is represented as follows:

$$V_{act,k} = \frac{R \bullet T}{n \bullet \alpha_k \bullet F} \ln\left(\frac{J}{J_{0,k}}\right) \tag{5}$$

Besides these parameters, it must be also considered the influence of the bubbles in the $V_{act,k}$. The bubble coverage rate, named θ, is represented through the effective electrode surface area S_{effec} and the total electrode surface area S, as shown in Eq. 6.

$$\theta = \frac{S - S_{eff}}{S} \tag{6}$$

For the actual operation condition, it may be used the simplified semi-empirical model of the bubble coverage rate, as follows:

$$\theta = 0.023(J)^{0.3}\left(\frac{T}{T_{ref}}\frac{P_{ref}}{P}\right)^{\frac{2}{3}} \tag{7}$$

where T_{ref} represents the initial reference temperature, P_{ref} represents the initial reference pressure, and J is the current density. The calculation of the expression shown in Eq. 7 is detailed in Milewski et al. (2014), and Vogt and Balzer (2005).

Therefore, to estimate the activation overpotential considering the bubble coverage rate, it is considered Eq. (8).

$$V_{act,k,\theta} = \frac{R \bullet T}{n \bullet \alpha_k \bullet F} \ln\left(\frac{J}{J_{0,k}}\right) + \frac{R \bullet T}{n \bullet \alpha_k \bullet F} \ln\left(\frac{1}{1-\theta}\right) \tag{8}$$

Hu et al. (2022) point out that the modeling shown below is in a quite mature stage, however, the main difficulty is to determine experimentally the activation overpotential.

During the electrolysis process, the electron migrates through several cells that are in parallel. The electron pass through the cathode, where a reduction reaction occurs, after that a hydroxide ion is generated, and it pass in the electrolyte and crossover from the diaphragm towards the anode, to the oxidation reaction. While this process is occurring, the lost electrons of the reaction will be passing through the polar frame to the next cell. Based on the explanation before, the ohmic resistance cab be divided in the cathode resistance (R_c), anode resistance (R_a), electrolyte resistance (R_{elect}), bubble resistance (R_{bubble}), and diaphragm resistance (R_{mem}). The Equation 9 indicates the ohmic resistance in the AWE.

$$V_{ohm} = (R_c + R_a + R_{ele} + R_{mem} + R_{bubble}) \bullet I \tag{9}$$

Preview results indicates that the ohmic loss changes almost linearly with the current density at a high current density, and is interesting to highlight that the ohmic resistance gas a dominant role in the overpotential (Hu et al. (2022)).

Because of irreversibilities (also named as overpotentials), the real cell voltage is always greater than the minimum voltage (reversible voltage according to the semi-reactions potential). Rodriguez and Amores (2020) list for the alkaline water electrolysis cell (AWE) the following overpotentials (i) Activation overpotentials: related to activation

energies of hydrogen and oxygen formation reactions on the surface of electrodes; (ii) Ohmic overpotentials: sum of the electrical resistance and the transport resistance related to gas bubbles, ionic transfer in the electrolyte, and resistivity of the diaphragm; (iii) Concentration overpotentials: due to mass-transport limitations occurring on the surface of the electrodes at high currents. The contribution of these overpotentials for hydrogen and oxygen gas generation is shown in the polarization curve of an electrolysis cell, in Figure 3. As represented in Figure 3, the higher the current density the greater the ohmic, H_2, and O_2 overpotentials at a constant temperature of 348 K.

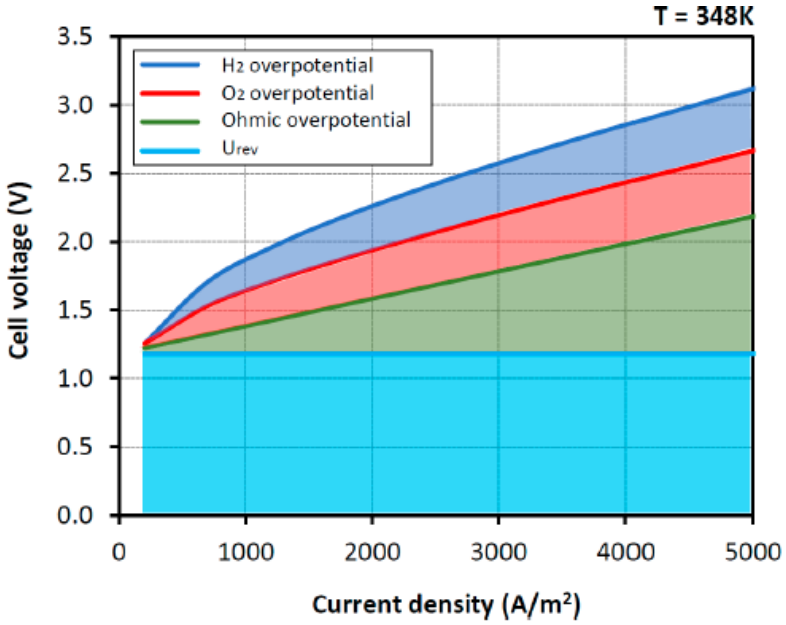

Figure 3 - Representation of a polarization curve, which correlates the cell voltage and current density at a constant temperature of 348 K. (Rodriguez and Amores, 2020)

2.3 THERMAL

The temperature during the electrolysis can affect the cell voltage, energy consumption, and also the gas purity. Despite the temperature gradient during the operation, it is allowable to consider a uniform temperature distribution in the electrolyzer, due to the fact that the heat transfer inside the control volume is higher compared with the convective heat transfer with the surroundings (Hu et al, 2022).

To model this process it considered the method of the lumped thermal capacitance to determine an equilibrium relationship between heat generation and dissipation, as shown in Eq. (10).

$$C_t \frac{dT}{dt} = \dot{Q}_{gen} - \dot{Q}_{loss} - \dot{Q}_{cool} - \dot{Q}_{exch} \tag{10}$$

where $\dot{Q}_{gen}$ represents the heat generation rate, $\dot{Q}_{loss}$ indicates the heat loss rate to the ambient, $\dot{Q}_{cool}$ represents the heat loss rate caused by electrolyte, $\dot{Q}_{exch}$ indicates the heat exchange rate, C_t is the overall thermal capacity of electrolyzer. As reported in the literature, Dieguez et al. (2008) proposed a calculation method by obtaining a series of heating curves experimentally under the condition of thermal insulation and no cooling water flow of electrolyzer. The calculation is as represented in Eq. (11).

$$C_t \approx \frac{P_{heat}}{dT/dt} \tag{11}$$

Jang et al. (2021) show a numerical model regarding the effect of temperature on the operational parameters of the water electrolyzer. The simulation results show that higher operating temperature increases the system efficiency only in the relatively high current density region (> 0.6 A/m²). The model developed in this study can be used to find the optimal configuration and operating condition of the AWE system.

2.4 GAS PURITY

The hydrogen and oxygen gas are formed in the electrolysis process, first, it is released in a dissolved state in the electrolyte, until it reaches the saturation state when it aggregates and grows at the electrode, and finally forms bubbles. After that, the bubbles may be carried by the flow, or cross the diaphragm interface. Due to the particular characteristics of the hydrogen gas such as being a better dissolver than oxygen and also having a higher molecular diffusion coefficient, it has a higher diffusion rate through the diaphragm. So, to obtain the gas impurity it is measured the hydrogen content in oxygen (HTO) at the anode side. A high HTO may cause safety problems and affect operation parameters as the Faraday efficiency and load range shrink.

To better understand the structure of the gas purity model, Hu et al (2022) developed Figure 2, which shows the model components of gas mixing and gas crossover, and this last one is interconnected with gas diffusion and gas convection. In addition, it is also shown the characteristic parameters and operating conditions of the numerical influence factors for each model component.

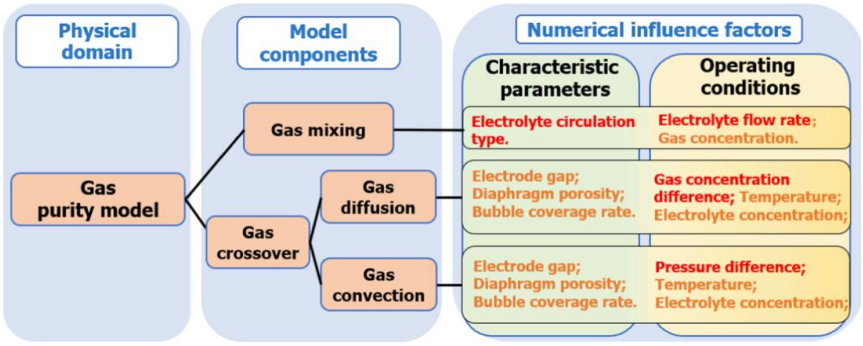

Figure 2. Gas purity model guide (Hu et al., 2022).

The gas purity model for the steady-state is performed based on classical gas-liquid reactors, considering the material balance relationship inside the reactor/electrolyzer. In order to simplify the modeling, a few assumptions are considered, such as during the reaction process only gas dissolved passes in the diaphragm, there is no phase transformation in the liquid pipeline, and the bubble in the gas-liquid separator can be completely separated.

The equations for the model of steady-state liquid substance are shown below in Eq. (12) and (13), and the gas substance balance in Eq. (14).

$$\text{Anode:} \quad \dot{V}_L^{ano} \bullet \left(c_{in,i}^{ano} - c_{out,i}^{ano}\right) + N_{phys,i}^{ano} \bullet A_{GL}^{ano} + N_{cross,i} \bullet A_m + (1 - f_{G.i}) \bullet \dot{n}_{R,i}^{ano} = 0 \tag{12}$$

$$\text{Cathode} \quad \dot{V}_L^{cat} \bullet \left(c_{in,i}^{cat} - c_{out,i}^{cat}\right) + N_{phys,i}^{cat} \bullet A_{GL}^{cat} + N_{cross,i} \bullet A_m + (1 - f_{G.i}) \bullet \dot{n}_{R,i}^{cat} = 0 \tag{13}$$

$$\frac{\dot{V}_G^j}{R \bullet T}\left(P_{in,i}^j - p_{out,i}^j\right) - N_{phys,i}^j \bullet A_{GL}^j + f_{G,i} \bullet \dot{n}_{R,i}^j = 0 \tag{14}$$

where i is the species type, j is the electrolyzer component type (anode or cathode), ${\dot{V}_L}^j$ is electrolyte flow rate, ${\dot{V}_G}^j$ is flow rate of gas output from electrolyzer, ${c_{in,i}}^j$ and ${c_{out,i}}^j$ represents the concentrations of dissolved gas in electrolyzer inlet and outlet respectively, ${P_{in,i}}^j$ and ${P_{out,i}}^j$ represents the partial pressure of electrolyzer inlet and outlet, respectively. The ${N_{phys,i}}^j$ indicates the desorption/absorption flux between liquid and gas phase, ${A_{GL}}^j$ indicates the overall interfacial area between the liquid and gas phase, $N_{cross,i}$ indicates the flux density of gas permeation through diaphragm, $f_{G,i}$ indicates the gas evolution efficiency, ${\dot{n}_{R,i}}^j$ is the molar flow rates of the species generated at electrodes. It must be highlighted that for the gas present in the input electrolyte it is considered in the dissolved state without a bubble, in other words, the partial pressure is zero for the inlet gas.

The steady-state gas purity equation showed above can represent only the gas purity at the outlet of electrolyzer stack. However, a dynamic analysis of impurity may be required to predict the gas purity at the outlet of the electrolysis system. As reported in the literature by Qi et al. (2021) a dynamic impurity model may accurately describe the variation of HTO with time. The dynamic impurity model can be obtained by the Rasch transform as indicated in Eq. (15).

$$\Phi_{H_2}^{anode}(s) = \frac{n_{H_2}}{\dot{n}_{O_2}} \prod_{j=1}^{n} \frac{1}{s \bullet \left(s + \frac{1}{\tau_j}\right)} \tag{15}$$

where Φ is the gas purity, s represents a complex variable and τ_j is the time constant for the mass transfer processes corresponding to the inertia of the gas–liquid separator for both the lower and the upper part, cooler, scrubber, and so on. The calculation of τ_j depends if it is calculated for the lower or upper part and can be verified in Hu et al. (2022).

Sanchez et al. (2020) using an Aspen Plus software carried out simulations to investigate and optimize the performance of the alkaline electrolysis system for hydrogen production. The main parameters based on semi-empirical equations that describe the voltage cell were Faraday efficiency and gas purity as a function of the current. The current density simulated ranges from 0.1 to 0.5 A/cm². The main result of the simulation showed that increasing the operation temperature (from 60°C to 80°C) and reducing the pressure (from 8 to 5 bar) can improve the overall performance of the system.

Antoniou et al. (2022) developed a new mathematical model to simulate and optimize different electrolyzer technologies. The model can also be used to study the effects of different operating conditions on the performance of the electrolyzers. For the alkaline water electrolysis (AWE) the models compared in the literature review were Ulleberg (2003), Amores et al. (2016), and Schalenbach et al. (2017) models.

Besides the developed models with the approach of thermodynamic, electrochemical, thermal, and gas purity presented before, others authors have developed models from the perspective of the electrolyzer's components such the multi-physics model from Hammoudi (2012). This multi-physics model considers structural parameters such as geometry, materials and also its evolution depending on operating conditions, besides that the operational parameters of the electrolyzer as temperature, pressure, concentration, bulk bubbling and recovery rate of electrode surface by the bubble.

2.5 MODELING

Besides modeling, Computational Fluid Dynamics (FD) can also be used as a powerful tool to optimize the electrolysis reaction efficiency and the cell design through the fluid dynamic and electrochemical processes. A few authors have worked on the evolution of simulating the hydrogen generation process, and the most remarkable are pointed out below.

A simulation tool for an alkaline electrolyzer based on a physical model of an electrolytic cell and an electrical analogy using MATLAB, Simulink/ SimPowerSystems was developed by Henao et al. (2014). This model accounts for the electrodes' electrochemical properties, the thermodynamics of the reaction, and the electoral properties of the electrode plates, membrane, and electrolyte. As a result of the simulation, it describes the electrolyzer's physical and electrical performance, besides that estimates the operating current as function of voltage, temperature pressure and electrolyte concentration.

A model and simulation 1D with seven free model parameters between them are wettability factor, charge transfer coefficients, roughness factors, and reference exchange current densities were designed by Abdin et al. (2017). This simulation provided an interesting tool to determine the sensitivity of the polarization curve regarding the exchange current densities of the anode and cathode.

Rodriguez and Amores (2020) developed a model that involves transport equations for both liquid and gas phases as well as equations for the electric current conservation using COMSOfi software. It evaluated the electrical response through the polarization curve at different temperatures, electrolyte conductivity, and electrode-diaphragm distance, considering real cases. This model had good accuracy in simulating the changes in gas profiles along the cell, according to current density, electrolyte flowrate, and electrode-diaphragm distance.

Jang et al. (2020) developed a numerical model to simulate and analyze the temperature effect on the performance on the AWE. The results indicated at higher temperature an increase in the system efficiency for the range of high current density. It was considered the electrolyte flow rate to maintain the temperature gradient throughout the cell based on the temperature and current density, and it resulted the increase of the system efficiency when the temperature gradient was reduced in the electrolysis cell.

Lee et al. (2021) worked in a three-dimensional (3-D) transient numerical model considering the hydrogen and oxygen evolution reactions, which resulted in the species and charge transport through various AWE components. The main highlight of this work is that it shows the contribution of hydroxide ion diffusion towards the ohmic losses through porous electrodes and a porous separator at low and high electrolyte flow rates.

Besides the work presented in the literature, more work have to be done in order to enhance alkaline electrolyzer performance.

3. CONCLUSIONS

The complete alkaline electrolysis process in an electrolyzer can be quite complex, and mathematical modeling can be used to help understand the process, diagnose, and even improve efficiency and hydrogen generation. This paper reviewed alkaline water electrolysis modeling from the perspective of thermodynamic, electrochemical, thermal, and gas purity models.

The main conclusions are that the thermodynamic model is related to the properties of substances involved in the reaction, and it is also the basis of the other modeling analysis. This modeling is relatively complete. The electrochemical model is the core of the electrolysis, and it requires more experimental work to obtain more overpotential data to reduce uncertainty of the calibrating process. For the purity gas model, both steady-state and dynamic models present high accuracy, however it is not commonly used for gas crossover prediction under different diaphragm. These models require optimization for hydrogen content in oxygen control reduction. Lastly, the thermal model in the literature are quite few, requiring more studies about the heat management and temperature control strategies.

4. REFERENCES

Abdin Z, Webb C J, Gray E M. Modelling and simulation of an alkaline electrolyser cell. Energy 2017; 138 : 316 -331.

Antoniou A, Berastain A, Hernandez D, Clis C. Mathematical modelling of coupled and decoupled water electrolysis systems based on existing theoretical and experimental studies. IntJournal of Hydrogen Energy 2022; 47 : 17526 – 17543.

der R, Klein A N, Binder C, Hammes G, Parucker M L, Ristow Junior W. Metallurgical composition of particulate materials, self-lubricating sintered products and process for obtaining self-lubricating sintered products. Patent, United States Patent and Trademark Office, Registry number: US-9243313-B2, Publication date: 06 December 2016.

Dieguez P, Ursua A, Sanchis P, et al. Thermal performance of a commercial alkaline water electrolyzer: Experimental study and mathematical modeling. Int J Hydrogen Energy 2008; 33 (24) : 7338 – 54.

Jang D, Choi W, Cho H, , Cho WC, Kin C H, Kang, S. Numerical modeling and analysis of the temperature effect on the performance of an alkaline water electrolysis system. J Power Sources 2020; 506 : 230106.

Jang D, Cho H, Kang S. Numerical modeling and analysis of the effect of pressure on the performance of an alkaline water electrolysis system. Appl Energy 2021; 287 : 116554.

Hammoudi M, Henao C, Agbossou K, Dube Ym Doumbia M L. New multi-physics approach for modelling and design of alkaline electrolyzers. Int J Hydrogen Energy 2012; 37 (19) : 13895 – 913.

Henao C, Agbossou K, Hammoudi M, Dube Y, Cardenas A. Simulation tool based as a physics model and an electrical analogy for an alkaline electrolyser. J Power Sources 2014; 250 : 58 – 67.

Hu S, Guo B, Ding S, Yang F, Dang J, Liu B, Gu J, Ma J, Ouyang M. A comprehensive review of alkaline water electrolysis mathematical modeling. Applied Energy 2022; 327 : 120099.

Lee J, Alam A, Ju H. CFD modeling and experimental validation of an alkaline water electrolysis cell for hydrogen production. Int J Hydrogen Energy 2021; 46 : 13678 - 13690.

Milewski J, Guandalini G, Campanari S. Modeling an alkaline electrolysis cell through reduced-order and loss-estimate approaches. J Power Sources 2014; 269 : 203 – 11.

Qi R, Gao X, Lin J, Song Y, Wang J, qiu Y, Liu M. Pressure control strategy to extend the loading range of an alkaline electrolysis system. Int J Hydrogen Energy 2021; 46 (73) : 35997 – 6011.

Rodriguez J, Amores E. CFD modeling and experimental validation of an alkaline water electrolysis cell for hydrogen production. Processes 2020; 8 : 1634.

Sanchez M, Amores, E, Abad D, Rodriguez L, Clemente-jul C. Aspen Plus model of an alkaline electrolysis system for hydrogen production. Int J Hydrogen Energy 2020; 45 : 3916 - 3929.

Ulleberg Ø. Modeling of advanced alkaline electrolyzers: a system simulation approach. Int J Hydrogen Energy 2003; 28 (1) : 21 – 33.

Vogt H, Balzer R. The bubble coverage of gas-evolving electrodes in stagnant electrolytes. Electrochim Acta 2005;50 (10) : 2073 – 9.

Zeng K, Zhang D. Recent progress in alkaline water electrolysis for hydrogen production and applications. Prog Energy Combust Sci 2010; 36 (3) : 307 – 26.

5. **RESPONSIBILITY NOTICE**

The author(s) is (are) the only responsible for the printed material included in this paper.